Graphene-based, Frequency-Domain Self-Trigger for Low SNR Air Showers-induced Pulses

Laurenciu, Nicoleta Cucu; Timmermans, Charles; Cotofana, Sorin D.

DOI
10.1109/ISCAS56072.2025.11043446

Publication date
2025

Document Version
Final published version

Published in
ISCAS 2025 - IEEE International Symposium on Circuits and Systems, Proceedings

Graphene-based, Frequency-Domain Self-Trigger for Low SNR Air Showers-induced Pulses

Nicoleta Cucu Laurenciu*, Charles Timmermans*, Sorin D. Cotofana†
*High Energy Physics Department, IMAPP, Radboud University, The Netherlands.
†Quantum and Computer Engineering Department, Delft University of Technology, The Netherlands.
*{N.CucuLaurenciu, C.Timmermans}@science.ru.nl †{S.D.Cotofana}@tudelft.nl

2025 IEEE International Symposium on Circuits and Systems (ISCAS) | 979-8-3503-5683-0/25/$31.00 ©2025 IEEE | DOI: 10.1109/ISCAS56072.2025.11043446

***Abstract*—In this paper we introduce a frequency-domain pulse detection method that is suitable for in-situ implementation at detector-level, for low-power, self-triggered air shower detectors. We propose a graphene-based architecture, and demonstrate its correct operation by means of SPICE simulations. The utilized graphene-based devices operate at low supply voltage, consume low energy per spike, and exhibit small footprints, which are essential properties for large-scale, energy-efficient implementations. The proposed method is particularly effective for very low (Signal-to-Noise Ratio) SNR scenarios, and is broadband noise resilient up to a certain extent, and (Radio Frequency) RF narrowband noise agnostic. Comparison results against time-domain signal-over-threshold trigger indicates that the proposed method can outperform its counterpart in terms of trigger efficiency by up to $26\times$ and $47\times$, when using 1 and 2 frequency components, respectively, especially for very low SNR scenarios (up to $-42\,\mathrm{dB}$) where time-domain methods are largely impaired. Furthermore, the proposed method does not require RF filtering in advance, and can coexist with other noise pulses. Thus, high detection efficiency that goes in tandem with high purity (low number of false positives) becomes tenable with proposed approach.**

***Index Terms*—Pulse Detection, DCT, Self-Trigger, Large-Scale Array, Graphene, Spiking Neural Network, Air Shower, Autonomous Radio Detection**

I. Introduction

Fast, accurate, and energy efficient detection of Extensive Air Showers (EAS) signatures captured by radio antennas amid a pervasive noise background, is a critical desideratum for high-energy astro-particle physics experiments [1], [2]. Radio detectors, owing to their low cost, are particularly attractive for new large scale air shower observatories (e.g., hundreds or thousands of free standing detectors [3], [4], [5]) with increased sensitivity of cosmic rays, photons, and neutrinos. Nevertheless, the detectors viability is predicated upon efficient, on-line (in-situ, at the detector unit level) autonomous triggering (self-trigger) (i.e., pulse detection), with excellent background noise rejection. The in-situ, detector-level requirement poses additional challenges, foremost (i) restricted computational power which limits the complexity of triggering procedures for EAS signals identification, (ii) real-time triggering constraints, to keep pace with the high speed data acquisition capabilities, and (iii) low power consumption, as in-field radio detector units are generally solar powered.

Existing self-trigger approaches [3], [6], [7], [8], [9], typically detect the EAS-induced pulses in the time-domain, by means of signal amplitude above noise floor threhsold as discriminator. Nevertheless, such methods trade-off detection efficiency for purity, i.e., if a certain extent of EAS events pulses is to be detected, then significantly more noise pulses are detected as well. This yields an extremely high trigger rate to which anthropogenic RF noise pulses falsely triggered upon, are the largest contributor. Furthermore, a high trigger rate is rendered prohibitive outside small scale detector arrays, thus it is imperative to reduce the large body of triggered pulses to a reasonable amount that can be handled by the mainstream data transmission capabilities. Recent self-trigger approaches that aim to tackle the high trigger rate by improving the rejection ability of falsely triggered upon noise pulses, include templates matched to expected EAS pulses various specificities [10], [11], [12], and neural networks (deep, convolutional, etc.) [13], [14], [12]. While the signal-over-threshold methods are inexpensive in terms of computing and power consumption and they are the traditional triggering approach on-line (at the in-situ single detector unit level), the neural networks and templates matching-based methods, are computationally demanding and are thus better suited for ulterior off-line processing. Moreover, the on-line in-situ trigger approaches require additional processing apriori the actual triggering, i.e., filtering of impulsive, band limited Radio Frequency (RF) noise (e.g., TV stations, FM band, power lines, beacons, (military) communication satellites).

In this paper, we introduce a real-time frequency domain method for triggering on air shower induced radio pulses, and its graphene-based implementation. To this end, we propose to compact the radio pulses energy signature in a few frequency components and use them as detection discriminator. The proposed method relies on a real-valued cosine transform, and is suitable for self-triggering detector units. We introduce a graphene-based architecture, and demonstrate its correct operation by means of in SPICE simulations. The utilized graphene-based devices operate at low supply voltage ($200\,\mathrm{mV}$), consume low energy per spike (in the order of $10^{-5}\mathrm{pJ}$), and exhibits small footprints, which are essential properties for large-scale energy-efficient implementations. Comparison results against traditional time-domain signal-over-threshold trigger indicates that the proposed method outperforms its counterpart in terms of trigger efficiency by up to $26\times$ and $47\times$, when using 1 and 2 frequency components, respectively, especially for very low SNR scenarios (up to $-42\,\mathrm{dB}$), where time-domain methods are largely impaired and EAS pulses submerged in a strong noise floor become undistinguishable from the background. Furthermore, the proposed method does not require in advance RF filtering and can coexist with other noise pulses. Thus, high detection

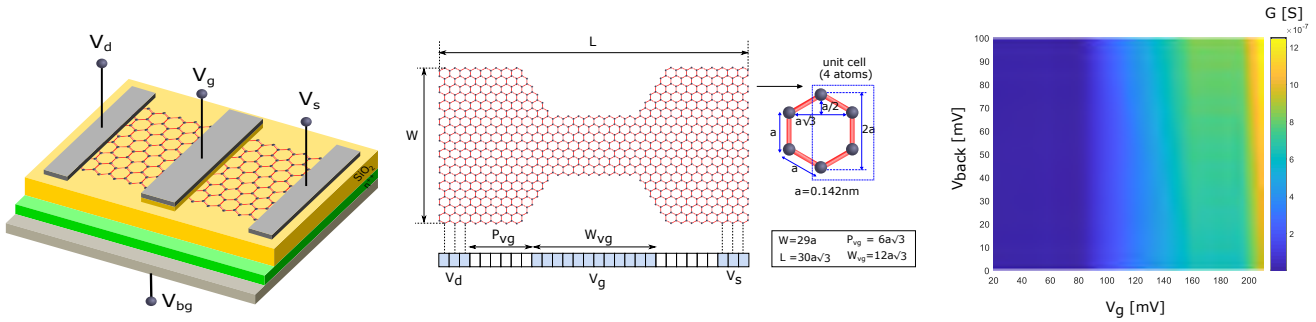

Fig. 1: Generic graphene-based device and conduction map example.

efficiency that goes along with high purity (low number of false positives) becomes tenable with the proposed approach.

II. Background

Figure 1 depicts the generic graphene device employed for the spiking neurons and synapses implementations [15], [16], [17], [18]. A Graphene NanoRibbon (GNR) forms the conduction channel when the device is subjected to drain-to-source voltage. The device conductance profile is modulated via external voltages applied on the top and/or bottom gates [19] and via varying the nanoribbon geometry and contact topology [20]. Note that all neurons and synapses utilized in this paper are GNR-based [15], [16]. Furthermore, GNR devices that can emulate periodic sine/cosine functions have been recently introduced [21] and can be utilized for continuous-time frequency domain processing.

As a measure of the noise level in the overall signal, we use Signal-to-Noise Ratio (SNR) measured in dB, defined as the ratio of the noise-free pulse power to the noise power, $SNR = 10\log_{10}\frac{P_{pulse}}{P_{noise}}$. A positive SNR implies the pulse amplitude is higher than the noise, while a negative SNR means the pulse is under the noise floor.

III. Frequency-Domain Pulse Triggering

To trigger in the frequency domain, one could exploit the energy content of the EAS pulses, which tends to be higher relative to the noise floor energy and spread across multiple frequencies in the Fourier domain. Thus, one could compute the energy based on the Fourier spectrum magnitude at a set of pulse-relevant frequencies, and use this as event pulses discriminator. From the computational standpoint, this approach requires to use both sines and cosines, and to compute L2 norm and possibly further calculations. Since we are targeting an in-situ self trigger methodology, for a viable solution we would thus like to reduce the computational complexity of the Fourier domain approach, and enhance its discrimination ability at the same time. To this end, in this paper, we propose an approach that relies on the Discrete Cosine Transform (DCT) (1), which uses an orthonormal basis of real-valued cosines only (instead of sines and cosines for Discrete Fourier Transform (DFT) (1), and concentrates most of the energy in only a few frequencies (instead of having the energy distributed across

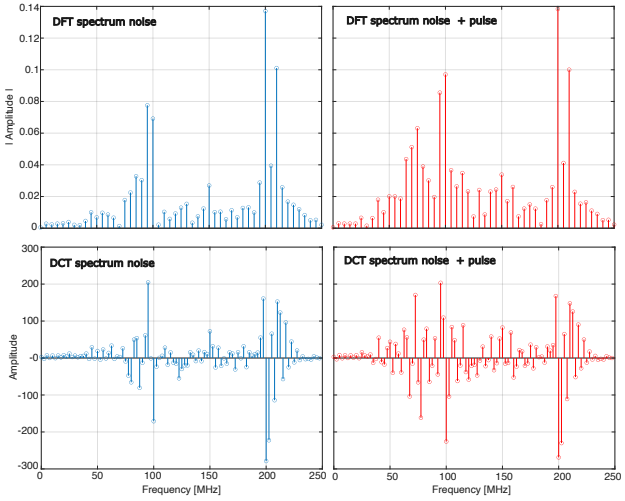

Fig. 2: DFT vs. DCT spectra for a noise only signal vs. same noise signal superimposed with an EAS pulse.

multiple frequencies for DFT).

$$X_k^{DFT} = \sum_{n=0}^{N-1} x_n \cdot cos\left[2\pi k\frac{n}{N}\right] - i\cdot\sum_{n=0}^{N-1} x_n \cdot sin\left[2\pi k\frac{n}{N}\right],$$
$$X_k^{DCT} = \sum_{n=0}^{N-1} x_n \cdot cos\left[\frac{\pi}{N}\left(n+\frac{1}{2}\right)k\right], \quad (1)$$

where N is the number of samples, and $k = 0 \ldots N-1$. Furthermore, due to the energy compaction property, we can use directly the DCT spectrum magnitude as discriminator instead of the energy, as it is already powerful enough. The DCT spectrum of noisy EAS pulses can be for instance orders of magnitude higher relative to the DCT noise spectrum, while the corresponding DFT spectrum is not. As an example, Figure 2 illustrates DFT and DCT spectra for a noise-only signal comparatively to the same noise trace to which one EAS pulse is superimposed. We can observe from the Figure that for the DFT case the magnitude for the noise + pulse is up to $5\times$ higher than the noise only DFT spectrum magnitude, while for the DCT case it is up to $180\times$ higher than the DCT noise-only spectrum. Additionally, it can be noticed in Figure 2 the spread-out distribution across the frequency spectrum for the DFT case, while for the DCT case there are only a few spectral

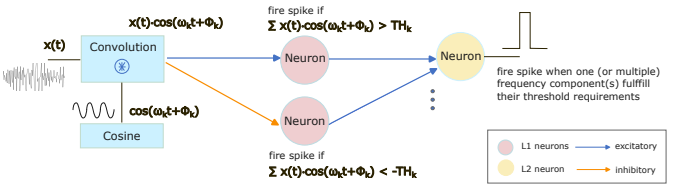

Fig. 3: Proposed frequency-domain trigger method architecture for one frequency component.

components with very high magnitude, concentrating most of the pulse energy. Thus, triggering in the cosine-based domain is more advantageous than in the Fourier domain.

We are now in position to formalize the proposed frequency-domain event pulse trigger criterium as:

$$Maj(|X_j^{DCT}| > TH_j) = \text{TRUE} \quad \text{then pulse trigger valid} \tag{2}$$

where j spans one or very few select frequencies (corresponding to the DCT components with the highest magnitude where the pulse energy is concentrated), TH_j denotes the threshold value for component X_j^{DCT} above which the magnitude should be. Essentially, a majority voter is applied to determine if the majority of the frequency components X_j^{DCT} each fulfilled their own TH_j threshold requirements, in which case a pulse trigger is deemed valid. We note that due to its energy compaction property the proposed method is particularly suited to deal with low SNR event pulses, where the time-domain triggering performs poorly or even fails altogether. Furthermore, for the proposed method the pulses frequency components can coexist with other known RF narrow band noise frequencies without affecting the triggering, as long as the triggered frequencies are clear. As a result, the RF filtering that precedes time-domain self-triggering is not necessary any longer, saving thus hardware resources and lowering the power consumption envelope.

IV. Graphene-based Implementation

Figure 3 illustrates the proposed frequency-domain pulse detection method architecture, for one frequency-domain component X_k^{DCT}. It consists of (i) a cosine generator block, that for given angular frequency ω_k and phase ϕ_k, outputs a continuous cosine wave $cos(\omega_k t + \phi_k)$, (ii) a convolution block, that receives as input the signal $x(t)$ comprising EAS pulses amid dominant background noise, and modulates the cosine amplitude with $x(t)$, (iii) 2 integrate and fire neurons (layer 1), that handle the time integration of $cos(\omega_k t + \phi_k)$ and evaluate whether $X_k^{DCT} > TH_k$ for positive X_k^{DCT} or $X_k^{DCT} < -TH_k$ for negative X_k^{DCT}, and (iv) one output integrate and fire neuron (layer 2), which generates a spike if the component $|X_k^{DCT}|$ was deemed to be above the threshold TH_k, signifying thus that a pulse was detected and triggered upon.

We note that a frequency component X_k^{DCT}, given by (1), can be either positive or negative. We account for this in the proposed architecture by using an excitatory synapse for the positive case and an inhibitory synapse for the negative case. For the excitatory synapse, small values at its input do not contribute almost at all; the bigger the value, the higher the influence for the synapse. For the inhibitory synapse, big values at its input do the most inhibition; the smaller the value, the higher the influence on the neuron membrane potential accumulation (and the less the inhibition). Thus, only one of the 2 neurons on layer 1 fire, accordingly to the X_k^{DCT} polarity.

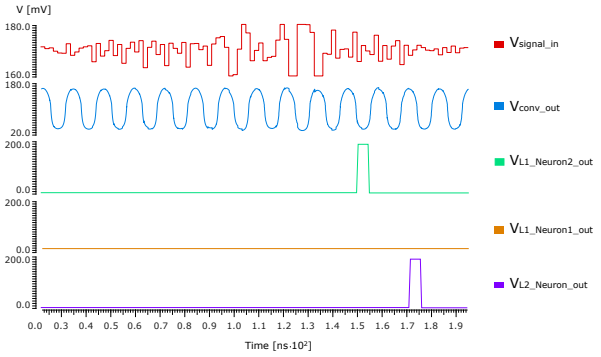

Fig. 4: Graphene-based frequency-domain pulse detection principle exemplification for one frequency component X_k^{DCT} at 70 MHz, over a time duration of 200 ns.

Figure 3 depicts the architecture for one frequency component. When extending the architecture to multiple k, the layer 2 output neuron is common to all X_k^{DCT} components, and serves as majority voter among them (i.e., if it receives spikes from the majority of components, then the pulse trigger is valid and it generates an output spike), while all the other architecture components (convolution and cosine blocks, and the 2 neurons on layer 1) are replicated for each k.

V. Simulation Results

Figure 4 illustrates the graphene-based frequency-domain trigger architecture operation for one frequency component X_k^{DCT}. When applying the input signal $V_{\text{signal\_in}}$ which is composed of noise superimposed with one EAS pulse (scaled within $[160, 180]$ mV), the convolution block generates as output the amplitude modulated cosine $V_{\text{conv\_out}}$. Further, the layer 1 neuron responsible with the positive thresholding of the time integrated frequency component X_k^{DCT}, generates no spikes at the output ($V_{\text{L1\_Neuron1\_out}}$), while the layer 1 neuron responsible with the negative thresholding of X_k^{DCT} generates a spike at the output ($V_{\text{L1\_Neuron2\_out}}$). In this example, only one X_k^{DCT} component was utilized and so, the layer 2 neuron responsible with the majority voting generates an output spike shortly after, signalling that a pulse was detected. An accurate evaluation of the area and energy consumption for the proposed architecture is not possible at this stage, however we can get some insight on these 2 aspects. For one frequency component, 3 neurons and 4 synapses are required, with a total area of $\approx 678\,\text{nm}^2$, and a total energy consumption in the order of 10^{-5}pJ for MHz frequency range [15].

In order to evaluate the performance of the proposed frequency-domain triggering method, we employ as metric the trigger efficiency defined as the ratio between the number of triggered EAS pulses via the algorithm, and the total number

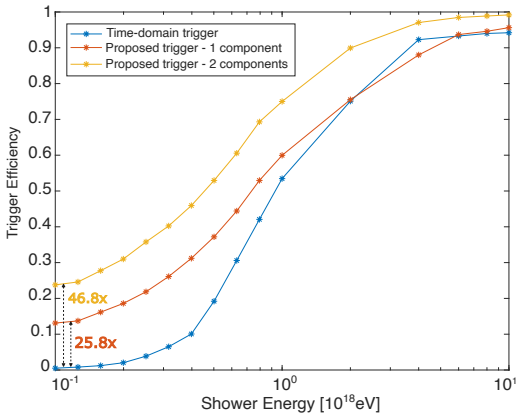

Fig. 5: Trigger efficiency vs. EAS showers energy.

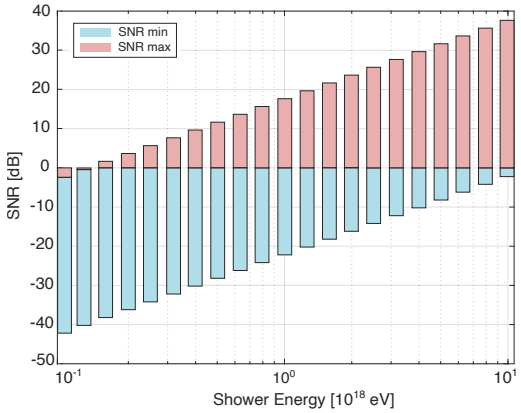

Fig. 6: SNR for considered EAS showers energy range.

of EAS pulses existing in the signal. As comparison reference, we consider the traditional time-domain signal-over-threshold triggering method. As concerns the simulation environment, the actual graphene-based frequency-domain trigger architecture is simulated in SPICE [22], while the determination of triggering threshold values for both methods, as well as the perfomance evaluation for the time-domain method are carried out in Matlab [23].

For generating relevant EAS pulses, a hydrogen nucleus was used as primary particle, with energies ranging from 10^{17} eV to 10^{19} eV. The produced air showers were simulated with geometries parameterized by zenith and azimuth angles, both ranging from $30°$ to $80°$. For every combination of primary energy, zenith angle and azimuth angle, 10 EAS events were generated. The simulation of particle cascade was carried out in AIRES [24], while the radio emission was computed via the ZHAireS extension [25]. The event pulses were then passed through realistic electronics response (e.g., antenna related, voltage gain, 20-200 MHz band-pass filtering). As background noise, synthetic mock-data that emulates the frequency spectrum of real noise traces similar to what can be expected in the Argentinian Pampas, was generated (100 traces of 50 million noise samples each, with a total duration of $0.1\,\mathrm{s}$ per noise trace). A $500\,\mathrm{MHz}$ signal acquisition sampling frequency was utilized, which is typical for current state-of-art Analog to Digital Converters (ADCs) used in radio-based air shower detectors.

For deriving the triggering thresholds for both methods, solely the noise-only traces are utilized. The trigger thresholds are then adjusted such that for each $0.1\,\mathrm{s}$ noise trace, a trigger rate of $100\,\mathrm{Hz}$ is generated (which corresponds to 10 triggered noise pulses in $0.1\,\mathrm{s}$). Once the threshold values were derived, we superimposed 10 EAS pulses randomly to each noise trace, and used the resulting signals as input to the triggering methods. Finally, we derived the trigger efficiency E for both proposed and time-domain triggering methods for showers in the energy range between 10^{17}eV to 10^{19}eV (which translates to EAS pulse amplitudes that are linearly scaled with the shower energy [26]). Figure 5 depicts the trigger efficiency results we obtained for the proposed method when using only one frequency component X_k^{DCT} ($145\,\mathrm{MHz}$), and when using 2 frequency components ($145\,\mathrm{MHz}$, and $120\,\mathrm{MHz}$), relative to the time-domain trigger method. The corresponding min and max SNR values for considered range of energies are displayed in Figure 6. Figure 5 reveals that the trigger efficiency of the proposed method outperforms the time-domain counterpart by up to $26\times$ for 1 frequency component and by up to $47\times$ for 2 frequency components. One can observe that for low SNR cases when EAS pulses are submerged in noise (low shower energy and thus low EAS pulse amplitude), the time-domain method performs poorly with a low trigger efficiency, while the proposed frequency-domain method is able to correctly detect such pulses. Furthermore, for very high SNR cases, the time-domain trigger efficiency is not 1 as one would expect, because the EAS pulses are corrupted by noise pulses. The time-domain method cannot differentiate between noise pulse and EAS pulse in these situations, and requires beforehand RF filtering for known interfering frequencies. On the contrary, the proposed method can coexist with such interfering frequencies and furthermore, the noise pulses, regardless of their high amplitude, can still be differentiated from EAS pulses. As opposed to the time-domain method, the proposed frequency-domain trigger method will not have as caveat an increase in false positives detections when the trigger efficiency increases.

VI. Conclusions

In this paper we introduced a novel graphene-based frequency-domain pulse detection method for self-triggering, radio detectors. The method is suitable for in-situ implementation at detector-level. We demonstrated its correct functionality by means of SPICE simulations. Comparison results against traditional time-domain signal-over-threshold trigger indicate that the proposed method can outperform in trigger efficiency by up to $26\times$ and $47\times$, when using 1 and 2 frequency components, respectively, for very low SNR scenarios (up to $-42\,\mathrm{dB}$), where time-domain methods are largely impaired. Furthermore, the proposed method does not require RF filtering in advance, and can coexist with other noise pulses, benefitting pulse detection for higher SNR case as well. Thus, high detection efficiency that goes along with high purity (low number of false positives) becomes tenable.

REFERENCES

[1] Schröder, F. G., "Radio Detection of Cosmic-Ray Air Showers and High-Energy Neutrinos." *Progress in Particle and Nuclear Physics*, vol. 93, pp. 1–68, 2017. [Online]. Available: https://doi.org/10.1016/j.ppnp.2016.12.002

[2] Coleman, A., et al., "Ultra high energy cosmic rays - The intersection of the Cosmic and Energy Frontiers." *Astroparticle Physics*, vol. 149, p. 102819, 2023. [Online]. Available: https://doi.org/10.1016/j.astropartphys.2023.102819

[3] Álvarez-Muñiz, J., Alves Batista, R., Balagopal V., A., Bolmont, J., Bustamante, M., et al., "The Giant Radio Array for Neutrino Detection (GRAND): Science and design." *Science China Physics, Mechanics and Astronomy.*, vol. 63, no. 1, p. 219501, 2020. [Online]. Available: https://doi.org/10.1007/s11433-018-9385-7

[4] Aab, A., et al., "The Pierre Auger Cosmic Ray Observatory." *Nuclear Instruments and Methods in Physics Research Section A: Accelerators, Spectrometers, Detectors and Associated Equipment (NIM-A).*, vol. 798, pp. 172–213, 2015. [Online]. Available: https://doi.org/10.1016/j.nima.2015.06.058

[5] Kawai, H., et al., "Telescope Array Experiment." *Nuclear Physics B - Proceedings Supplements.*, vol. 175-176, pp. 221–226, 2008. [Online]. Available: https://doi.org/10.1016/j.nuclphysbps.2007.11.002

[6] Kelley, J. L., et al., "Data Acquisition, Triggering, and Filtering at the Auger Engineering Radio Array." *Nuclear Instruments and Methods in Physics Research Section A: Accelerators, Spectrometers, Detectors and Associated Equipment (NIM-A).*, vol. 725, pp. 133–136, 2013. [Online]. Available: https://doi.org/10.1016/j.nima.2012.11.153

[7] Monroe, R., et al., "Self-triggered radio detection and identification of cosmic air showers with the OVRO-LWA." *Nuclear Instruments and Methods in Physics Research Section A: Accelerators, Spectrometers, Detectors and Associated Equipment (NIM-A).*, vol. 953, p. 163086, 2020. [Online]. Available: https://doi.org/10.1016/j.nima.2019.163086

[8] Charrier, D., et al., "Autonomous radio detection of air showers with the TREND50 antenna array." *Astroparticle Physics.*, vol. 110, pp. 15–29, 2019. [Online]. Available: https://doi.org/10.1016/j.astropartphys.2019.03.002

[9] Bezyazeekov, P. A., et al., "Measurement of cosmic-ray air showers with the Tunka Radio Extension (Tunka-Rex)." *Astroparticle Physics.*, vol. 802, pp. 89–96, 2015. [Online]. Available: https://doi.org/10.1016/j.nima.2015.08.061

[10] Barwick, S. W., et al., "Radio Detection of Air showers with the ARIANNA Experiment on the Ross Ice Shelf." *Astroparticle Physics*, vol. 90, pp. 50–68, 2017. [Online]. Available: https://doi.org/10.1016/j.astropartphys.2017.02.003

[11] Henrichs, J., et al., "Searching for Air Showers with RNO-G." in *Proceedings of 9th International Workshop on Acoustic and Radio EeV Neutrino Detection Activities (ARENA)*, vol. 424, 2019, p. 007. [Online]. Available: https://doi.org/10.22323/1.424.0007

[12] Correa, P., et al., "Development of an Autonomous Detection-Unit Self-Trigger for GRAND." in *Proceedings of 10th International Workshop on Acoustic and Radio EeV Neutrino Activities (ARENA)*, 2019.

[13] Führer, F., et al., "Towards online triggering for the radio detection of air showers using deep neural networks." in *Proceedings of 8th International Conference on Acoustic and Radio EeV Neutrino Detection Activities (ARENA)*, 2019, p. 03004. [Online]. Available: https://doi.org/10.1051/epjconf/201921603004

[14] Le Coz, S., et al., "Identification of air-shower radio pulses for the GRAND online trigger." in *Proceedings of 38th International Cosmic Ray Conference (ICRC)*, vol. 444, 2019, p. 224. [Online]. Available: https://doi.org/10.22323/1.444.0224

[15] Wang, H., Cucu Laurenciu, N., and Cotofana, S. D., "A Reconfigurable Graphene-Based Spiking Neural Network Architecture." *IEEE Open Journal of Nanotechnology*, vol. 2, pp. 59–71, 2021. [Online]. Available: https://doi.org/10.1109/OJNANO.2021.3094761

[16] Wang, H., Cucu Laurenciu, N., Jiang, Y., and Cotofana, S. D., "Ultra-Compact, Entirely Graphene-Based Nonlinear Leaky Integrate-and-Fire Spiking Neuron." in *IEEE International Symposium on Circuits and Systems (ISCAS)*, 2020, pp. 1–5. [Online]. Available: https://doi.org/10.1109/ISCAS45731.2020.9181092

[17] Cucu Laurenciu, N., Timmermans, C., and Cotofana, S. D., "Low Energy, Non-Cortical, Graphene Nanoribbon-Based STDP Plastic Synapses." *Astroparticle Physics.*, vol. 16, no. 6, pp. 4–13, 2022. [Online]. Available: https://doi.org/10.1109/MNANO.2022.3208722

[18] Wang, H., Cucu Laurenciu, N., Jiang, Y., and Cotofana, S. D., "Graphene-Based Artificial Synapses with Tunable Plasticity." *ACM Journal on Emerging Technologies in Computing Systems (JETC).*, vol. 17, no. 50, pp. 1–21, 2021. [Online]. Available: https://doi.org/10.1145/3447778

[19] Cotofana, S. D., Dimitrakis, P., Enachescu, M., Karafyllidis, I., Rubio, A., and Sirakoulis, G. C., "On graphene nanoribbon-based nanoelectronic circuits viability." in *42nd Workshop Compound Semicond. Devices Integr. Circuits Held Eur.*, 2018, pp. 35–36.

[20] Jiang, Y., Cucu Laurenciu, N., and Cotofana, S. D., "On Basic Boolean Function Graphene Nanoribbon Conductance Mapping." *IEEE Transactions on Circuits and Systems-I: Regular Papers.*, vol. 66, no. 5, pp. 1948–1959, 2018. [Online]. Available: https://doi.org/10.1109/TCSI.2018.2882310

[21] Verton, P., et al., "Graphene Nanoribbon-based Analog-to-Digital Conversion." in *Proceedings of 24th IEEE International Conference on Nanotechnology (NANO)*, 2024, pp. 580–585. [Online]. Available: https://doi.org/10.1109/NANO61778.2024.10628546

[22] Cadence. [Online]. Available: https://www.cadence.com/.

[23] Matlab. [Online]. Available: https://www.mathworks.com/.

[24] Sciutto, S. J., Knapp, J., Capdevielle, J. N., Schatz, G., and Thouw, T., "AIRES: A System for Air Shower Simulations." 2002.

[25] Álvarez-Muñiz, J., Carvalho, Jr. W. R., Tueros, M., and Zas, E., "Coherent Cherenkov radio pulses from hadronic showers up to EeV energies." *Astroparticle Physics.*, vol. 35, no. 6, pp. 287–299, 2012. [Online]. Available: https://doi.org/10.1016/j.astropartphys.2011.10.002

[26] Aab, A., et al., "Measurement of the radiation energy in the radio signal of extensive air showers as a universal estimator of cosmic-ray energy." *Physical Review Letters.*, vol. 116, no. 24, p. 241101, 2016. [Online]. Available: https://doi.org/10.1103/PhysRevLett.116.241101